International Journal of Thermal Sciences 48 (2009) 2017–2024

Contents lists available at ScienceDirect

International Journal of Thermal Sciences

journal homepage: www.elsevier.com/locate/ijts

Large Eddy simulation of turbulent mixed convection in a 3D ventilated cavity: Comparison with existing data

Ridouane Ezzouhri [a], Patrice Joubert [a,*], François Penot [b], Sophie Mergui [c]

[a] LEPTIAB, Université de La Rochelle, Av. Michel Crépeau, 17042 La Rochelle cedex 1, France
[b] LET-ENSMA, UMR CNRS 6608, BP 40109, 86961 Futuroscope cedex, France
[c] Laboratoire Fluides Automatique et Systèmes Thermiques (FAST), UMR CNRS 7608, Campus Universitaire – Bât. 502, 91405 Orsay cedex, France

ARTICLE INFO

Article history:
Received 22 January 2008
Received in revised form
29 March 2009
Accepted 30 March 2009
Available online 6 May 2009

Keywords:
Turbulent mixed convection
Indoor airflow
Large Eddy Simulation
Dynamic subgrid-scale model
Flow bifurcation
Hysteresis cycle

ABSTRACT

We consider in this study the mixed convection airflow encountered in a 3D anisothermal cavity ventilated with supply and exhaust slots under stable thermal stratification. The flow in this cavity has been experimentally studied in the past (S. Mergui, Caractérisation expérimentale des écoulements d'air de convection naturelle et mixte dans une cavité fermée, thèse de l'Université de Poitiers, France, 1993) and was subject to a jet deflection and to a sudden change in the flow pattern between a general clockwise rotation and a counter-clockwise rotation when varying the inlet jet velocity. This phenomenon also exhibits a hysteresis effect depending on the way the velocity is changed, which made us to think that this flow bifurcation is of subcritical nature. Numerical studies have been yet devoted to this configuration, using RANS simulations or Large Eddy Simulation (LES), but this phenomenon has not been reported. So, we chose to numerically study this challenging flow with an LES approach associated with a subgrid diffusivity model previously developed for natural convection airflows. The comparison with the available experimental data and with other LES results using a classical dynamic model proves that the present LES not only correctly predicts the mean characteristics of the flow but is also able to correctly reproduce the flow bifurcation and the hysterisis effect.

1. Introduction

We are interested in this paper with numerical simulations of indoor airflows under mixed convection situations. Because air distribution inside a room results from buoyancy effects due to temperature differences (natural convection), momentum differences due to mechanical ventilation system (forced convection) or external pressure differences on the facades of the room, many indoor situations experience mixed convection flows. As a wide variety of flow structures can be encountered depending on the local and instantaneous equilibrium between inertial and buoyancy forces, combining as an example laminar to turbulent transition, relaminarisation, detached or recirculating flow regions, mixed convection is a very challenging field of research for Computational Fluid Dynamics on the one hand, and for engineering and economical purposes such as building ventilation systems design, energy saving or comfort improvement on the other hand.

From a computational point of view, indoor airflows have been investigated extensively in the past decades, particularly for turbulence modelling. Nevertheless, most of the work is devoted to forced convection flows in isothermal ventilated enclosures such as the one experimentally studied during Annex 20 of the International Energy Agency by Nielsen [1] which constitutes a benchmark exercise for numerous turbulence model adjustments (see as an example Refs. [2–5]).

On the other hand, mixed convective flows have received comparatively less numerical attention. We will focus in this study on the case of a non-isothermal ventilated cavity experimentally investigated by Mergui during her Ph.D. thesis [6]. Despite this cavity is a reduced scale model rather than a real size room, it is very challenging. First, the airflow in this 1 m^3 cavity is representative of flow features encountered in real rooms and second the flow exhibits a singular behaviour when varying the inlet jet velocity, with a bifurcation between two turbulent clockwise and anti-clockwise airflow regimes associated to a hysteresis phenomenon.

Moreover, this cavity has been numerically studied by several authors using RANS or LES approaches [4,5,7–9]. Particularly, Chen and co-workers [4,5,9], commonly use this cavity as a test case for

* Corresponding author. Tel.: +33 05 46513901; fax: +33 05 46513939.
E-mail address: patrice.joubert@univ-lr.fr (P. Joubert).

1290-0729/$ – see front matter © 2009 Elsevier Masson SAS. All rights reserved.
doi:10.1016/j.ijthermalsci.2009.03.017

Nomenclature

Ar	Archimede number
Ax, Ay	aspect ratios of the cavity
C	constant of the subgrid model
D	depth of the cavity, m
Fr	Froude number
g	gravitational acceleration, m s^{-2}
G	filter function, m^{-1}
h_i	subgrid heat flux per unit of thermal mass ρc_p, K m s^{-1}
H	height of the cavity, m
Φ_{sm}	subgrid thermal energy per unit of thermal mass ρc_p, K m s^{-1}
h	height of the inlet slot, m
k	non-dimensional turbulent kinetic energy
l	height of the exhaust slot, m
P	modified pressure, m s^{-2}
Pr	Prandtl number
Ra	Rayleigh number
S_{ij}	strain-rate tensor, s^{-1}
Re	Reynolds number
t	time, s
T, ΔT	temperature and temperature difference, K
T_{ij}	subgrid thermal tensor, K m^{-1} s^{-1}
U	non-dimensional horizontal velocity
U_{inj}	mean flow rate velocity at injection, m s^{-1}
W	cavity width or non-dimensional vertical velocity, m or –
x, y, z	non-dimensional Cartesian coordinates
y^+	wall units coordinate

Greek letters

ν	kinematic viscosity, m^2 s^{-1}
ρ	density, kg m^{-3}
θ, $\Delta\theta$	non-dimensional temperature and temperature difference
κ	thermal diffusivity m^2 s^{-1}
τ_{ij}	subgrid stress tensor, m^2 s^{-2}
Δ	filter width, m

Subscripts

air	relative to air properties
h	relative to the inlet slot
H	relative to the height of the cavity
mol	relative to non-dimensional molecular quantities
sm	relative to subgrid quantities

Superscripts

$\overline{x}$	implicit filtered variables
$\widetilde{x}, \widehat{x}$	explicit filtered variables

different versions of RANS or LES models. In this way, Xu and Chen [9] using a 2D RANS approach with a modified two-layer model observed a good agreement with the experimental data for the clockwise flow pattern. They also observed the anti-clockwise pattern, but this case was not well documented. Previously, Zhang and Chen [4] investigated the flow in this cavity with two LES models, a classical Smagorinsky model, and a Filtered Dynamic Scale Model. However, their results, obtained on a coarse $62 \times 12 \times 62$ grid were not really convincing. Recently, Zhang et al. [5] revisited this problem performing a comparison not only between various RANS models but also between LES and DES, and obtained a satisfactorily comparison between LES and the experimental data for the mean and turbulent clockwise fields, using a $60 \times 30 \times 60$ spatial grid.

Nevertheless, none of these numerical studies report the hysteresis cycle associated to the flow bifurcation, so we chose to numerically explore this cavity with an original LES approach. LES is preferred here because it avoids DNS spatial requirements, and contrarily to RANS modelling, LES is a naturally unsteady description which allows to access not only the statistic quantities but also the instantaneous pictures of the flow as can be obtained during a real experiment.

Various viscosity subgrid-scale models have been developed for LES in the last 40 years, the first and simple one being the Smagorinsky model [10] and the currently more popular one being the dynamic Germano–Lilly model [11, 12]. In this paper, we use an original subgrid diffusivity model based on the thermal characteristics of the flow, which avoids to consider a subgrid Reynolds analogy generally encountered in LES studies of natural convection flows. This original "Mixed Scales Diffusivity Model" proved to be efficient when applied to pure natural convection problems at high Rayleigh numbers [13–15] and we investigate here its capability to deal with mixed convection flows in cavities.

First, we briefly present the description of the LES approach and the subgrid-scale modelling, followed by the description of the numerical procedure. Afterwards, the physical problem is presented and a description of the observed airflow behaviour in the experimental cavity is given.

The numerical results obtained with the Mixed Scale Diffusivity Model associated to a dynamic procedure are then compared with the experimental data available in Refs. [6–8] and also with the recent LES results of Zhang et al. [5], as this later paper probably provides the actually best available LES results for this cavity.

Finally, the numerical investigation of the flow bifurcation associated to the hysteresis effect is presented and discussed.

2. LES approach

The LES separates small-eddies from large-eddies with a spatial convolution filtering. For one-dimensional flow, the filtered velocity is:

$$\overline{u}_i = \int G(x, x') u_i(x') \mathrm{d}x' \tag{1}$$

where $G(x, x')$ is a filter function. The filter function value is large only when $(x - x')$ is less than the filter width, a length scale over which averaging is performed. The eddies larger than the filter width are called the "large-eddies", and the eddies smaller than the filter width are the "small-eddies". In the physical spaces, a box filter is usually used, i.e.:

$$G(x_i) = \begin{cases} 1/\Delta_i & (|x_i| \le \Delta_i/2) \\ 0 & (|x_i| > \Delta_i/2) \end{cases} \tag{2}$$

When performing finite-volume method, it seems natural to define the filter width, Δ_i, as an average over a grid volume. For a three-dimensional flow, the filter width is generally defined as $\Delta = (\Delta x \Delta y \Delta z)^{1/3}$, where Δx, Δy and Δz are, respectively, the sizes of the control volume in the *X*, *Y* and *Z* directions.

When dealing with non-isothermal flows in ventilated cavities, application of the filtering technique to the equations of motion

and energy under Boussinesq's assumption lead to the following non-dimensional equations:

$$\begin{aligned}
&\frac{\partial \overline{u}_i}{\partial x_i} = 0\\
&\frac{\partial \overline{u}_i}{\partial t} + \frac{\partial (\overline{u}_i \overline{u}_j)}{\partial x_j} = -\frac{\partial \overline{P}}{\partial x_i} + \frac{\partial}{\partial x_j}(2\nu_{\mathrm{mol}} \overline{S}_{ij}) - \frac{\partial \tau^d_{ij}}{\partial x_j} + \frac{Ra_{\mathrm{H}}}{Pr \times Re^2_{\mathrm{H}}} \overline{\theta} \delta_{iZ}\\
&\frac{\partial \overline{\theta}}{\partial t} + \frac{\partial (\overline{\theta} \overline{u}_j)}{\partial x_j} = \frac{\partial}{\partial x_j}\left(\kappa_{\mathrm{mol}} \frac{\partial \overline{\theta}}{\partial x_j}\right) - \frac{\partial h_j}{\partial x_j}
\end{aligned} \tag{3}$$

where $\overline{(\_)}$ denotes the filtered variables.

These equations are made dimensionless by using the cavity height, H, as the reference length and the mean supply air velocity, U_{inj}, as reference velocity. The dimensionless temperature θ is defined as $\overline{\theta} = (\overline{T} - T_0)/\Delta T$ where ΔT is a characteristic temperature difference around the reference temperature T_0 (in our case, ΔT will the difference between the hot and the cold walls, $\Delta T = (T_{\mathrm{h}} - T_{\mathrm{c}})$ and T_0 the mean temperature). $\overline{S}_{ij} = 0.5(\partial \overline{u}_i/\partial x_j + \partial \overline{u}_j/\partial x_i)$ is the strain-rate tensor based on the resolved velocity field. Ra_{H} and Re_{H} are, respectively, the Rayleigh and the Reynolds numbers based on the cavity height. Pr is the Prandtl number while $\nu_{\mathrm{mol}} = Re_{\mathrm{H}}^{-1}$ and $\kappa_{\mathrm{mol}} = (Pr \times Re_{\mathrm{H}})^{-1}$ are, respectively, the dimensionless molecular viscosity and diffusivity. The ratio between the buoyant and inertial effects $Ra_{\mathrm{H}}/(Pr \times Re^2_{\mathrm{H}})$ defines the Archimede number, Ar, (also called Richardson number), and the Froude number is defined in turn as $Fr = Ar^{-1/2}$.

3. Subgrid-scale modelling

The effects of the subgrid-scales on the resolved quantities are accounted by the subgrid-scale stress quantities:

$$\begin{aligned}
\tau_{ij} &= \overline{u_i u_j} - \overline{u}_i \overline{u}_j\\
h_j &= \overline{\theta u_j} - \overline{\theta} \overline{u}_j
\end{aligned} \tag{4}$$

which need to be modelled.

The deviatoric part of the subgrid stress tensor, τ^{d}_{ij}, is generally modelled through an eddy viscosity model, first proposed by Smagorinsky [10], based on the resolved strain-rate tensor $\overline{S}_{ij}$:

$$\tau^{\mathrm{d}}_{ij} = \tau_{ij} - \frac{1}{3}\tau_{kk}\delta_{ij} = -2\nu_{\mathrm{sm}} \overline{S}_{ij}, \tag{5}$$

where ν_{sm} is the subgrid eddy viscosity. The isotropic part of the subgrid stress tensor, τ_{kk}, is included in the modified filtered pressure $\overline{P}$.

In the same way, the subgrid heat flux h_j can be related to the large-scale temperature gradient by an eddy diffusivity, κ_{sm}, as:

$$h_j = -\kappa_{\mathrm{sm}}(\partial \overline{\theta}/\partial x_j) \tag{6}$$

In most of the subgrid-scale models used in natural convection flows, the subgrid-scale diffusivity κ_{sm} is deduced from the subgrid-scale viscosity ν_{sm}, assuming a Reynolds analogy ($\kappa_{\mathrm{sm}} = \nu_{\mathrm{sm}} Pr^{-1}_{\mathrm{sm}}$) with the introduction of a subgrid Prandtl number which can be either a constant or a time and space varying parameter obtained through a dynamic approach [11, 12]. This, in fact amounts to consider that the small thermal scales depend solely on the resolved dynamic scales, which is suspected not to hold in the case of turbulent natural convection, where the flow is produced by buoyant forces and not through a dynamic forcing.

In this study, we choose to use a different way in modelling the subgrid diffusivity, with the Mixed Scale Diffusivity Model (MSDM) initially developed for natural convection flows in cavities by Sergent et al. [13]. In this model, whose complete derivation can be found in [13], κ_{sm} is not related to the subgrid viscosity but is obtained along two different but complementary approaches: first a Smagorinsky like model that extracts information from the thermal resolved scales, second a model based on the thermal energy of the subgrid-scales, following the TKE model of Bardina for the subgrid viscosity [16]. This complete MSDM diffusivity model then reads:

$$\kappa_{\mathrm{sm}} = C_{\mathrm{model}} \left(\frac{\overline{\Delta}^3}{\Delta\theta} |\overline{T}|^{1/2}\right)^{1/2} \left(\frac{\overline{\Delta}}{\Delta\theta} (\Phi_{\mathrm{sm}})^{1/2}\right)^{1/2} \tag{7}$$

with $|\overline{T}| = 2\overline{T}_{ij}\overline{T}_{ij}$ and $\overline{T}_{ij} = \overline{S}_{ij}\partial\overline{\theta}/\partial x_j$ (no summation on i and j). Φ_{sm} stands for the subgrid thermal energy, which can be estimated at the spatial cut-off following the Bardina similarity hypothesis [16] as $\Phi_{\mathrm{sm}} = 0.5(\overline{u}_i - \widehat{\overline{u}}_i)(\overline{\theta} - \widehat{\overline{\theta}})$. Variables $\widehat{\overline{u}}_i$ and $\widehat{\overline{\theta}}$ are, respectively, the doubly filtered velocity and temperature on an explicit test filter ($\widehat{\overline{\Delta}}$) different of the implicit filter ($\overline{\Delta}$). The subgrid-scale dependency of this model ensures that it vanishes in fully resolved regions of the flow and near the walls, and it has been successfully applied to various 3D natural convection flows [13–15].

The ability of the model to adapt itself to the local flow structure can be reinforced by the use of a dynamic approach, in order to define the value of the model coefficient C_{model} at each point of the grid. This is obtained through the dynamic procedure proposed by Germano et al. [11], whose general idea is that subgrid-scale quantities h_j and H_j corresponding to two different filters (the grid filter $\overline{\Delta}$, and an explicit test filter $\widetilde{\overline{\Delta}}$, generally twice larger than $\overline{\Delta}$), can be modelled with the same functional form on the two filtering levels. Germano applied this procedure to the Smagorinsky model in order to derive the original "dynamic model", but this dynamic procedure can be performed whatever subgrid model.

For the MSDM, the subgrid-scale heat flux attached to the implicit grid filter is:

$$h_j = \overline{\theta u_j} - \overline{\theta}\overline{u}_j = -C_{\mathrm{dyn}} \frac{\overline{\Delta}^2}{\Delta\theta} |\overline{T}|^{1/4} (\Phi_{\mathrm{sm}})^{1/4} (\partial\overline{\theta}/\partial x_j) \tag{8}$$

Similarly, the subgrid-scale heat flux on the explicit filtering level is:

$$H_j = \widetilde{\overline{\theta u_j}} - \widetilde{\overline{\theta}}\widetilde{\overline{u}}_j = -C_{\mathrm{dyn}} \frac{\widetilde{\overline{\Delta}}^2}{\Delta\theta} |\widetilde{\overline{T}}|^{1/4} \left(\widetilde{\Phi}_{\mathrm{sm}}\right)^{1/4} (\partial\widetilde{\overline{\theta}}/\partial x_j) \tag{9}$$

Assuming that the coefficient C_{dyn} is the same for the two filtering levels [11], it can be determined in each point through a least square minimization procedure proposed by Lilly [12] as:

$$C_{\mathrm{dyn}} = E_j Q_j / Q_j Q_j \tag{10}$$

where

$$Q_j = \left(\frac{\overline{\Delta}^2}{\Delta\theta} \left|\overline{T}\right|^{\frac{1}{4}} (\Phi_{sm})^{\frac{1}{4}} (\partial\overline{\theta}/\partial x_j)\right) - \frac{\widetilde{\overline{\Delta}}^2}{\Delta\theta} \left|\widetilde{\overline{T}}\right|^{\frac{1}{4}} (\widetilde{\Phi}_{sm})^{\frac{1}{4}} (\partial\widetilde{\overline{\theta}}/\partial x_j) \tag{11}$$

and

$$E_j = H_j - \widetilde{h}_j = \widetilde{\overline{\theta u}}_j - \widetilde{\overline{\theta}}\,\widetilde{\overline{u}}_j \tag{12}$$

The interest of the dynamic approach is that it locally adjusts the value of the subgrid model coefficient according to the local flow

patterns without modifying the subgrid-scale model. However, as C_{dyn} can locally become negative and unbounded, its variations must be clipped in order to avoid numerical instability.

4. Numerical procedure

The present 3D LES is based upon a structured Finite-Volume approach. The governing equations are integrated in time using a prediction–projection fractional time step algorithm for the velocity–pressure coupling. In the prediction step, the momentum equations (Navier–Stokes equations) are advanced in time using the known pressure at the previous time step. The time discretization is second-order accurate and combines a second-order backward Euler scheme for the time derivative, an implicit formulation for the diffusion terms and an explicit second-order Adams–Bashforth extrapolation for the nonlinear terms. The spatial discretization is achieved with a classical finite-volume method on staggered grids. The resulting Helmholtz equations are solved by an incremental ADI technique and the Poisson's equation for pressure correction is solved by partial diagonalization of the discrete operator of spatial derivatives. All the terms involved in the balance equations are evaluated with second-order accurate centered schemes, but a QUICK scheme is used for the nonlinear terms of the momentum equations. Using an a priori test, Sergent et al. [13] showed that the artificial dissipation induced by the QUICK approximation was able to correctly reproduce the energy transfer between the resolved and the unresolved scales of the flow in the case of natural convection. Therefore, we do not consider any explicit subgrid viscosity in the momentum equations (ν_{sm} is set to zero) and the subgrid-scale modelling lies only on the above presented dynamic subgrid-scale diffusivity model (Eqs. (7) and (10)) which is introduced in the energy equation. The numerical treatment of the energy equation is similar to the preceding one for the momentum equation, except for the nonlinear terms which are evaluated with a second-order centered scheme in order to avoid any numerical diffusion superimposed on the subgrid diffusivity model.

5. Experimental configuration

5.1. Description

The test case considered in this paper is the experimental anisothermal ventilated cavity investigated by Mergui et al. [6] and Blay et al. [7,8]. The experimental database includes charts of the mean values of velocity, temperature and turbulent kinetic energy in the mid-depth plane of the cavity and is well suited for CFD code validation. Although the configuration is a laboratory model rather than a real sized room, the induced mixed convection flow inside this cavity is representative of flow features found in real rooms and is numerically very challenging. The main flow is characterized by a horizontal anisothermal jet and thin boundary layers along the vertical walls that encircle an essentially isothermal core region.

The geometry of this experimental cavity is shown in Fig. 1. The height and the width of the cavity are $H = W = 1.04$ m. The total depth of the experimental setup is equal to 0.7 m, but the cavity is separated into three parts, with two lateral guard cavities and a central cavity of depth $D = 0.3$ m for measurements. The geometrical aspect ratios to consider are then $A_x = W/H = 1$ and $A_Y = D/H = 0.3$. Cold air at temperature $T_c = 15\,^{\circ}$C is horizontally discharged from a thin inlet slot of height $h = 0.018$ m at the ceiling level and the exhaust slot of height $l = 0.024$ m is located at the floor level on the opposite wall. The two slots extend through the whole width of the cavity in order to reduce the 3D effects in the cavity, and produce an approximately plane jet at the inlet. The floor is heated at temperature $T_h = 35\,^{\circ}$C, while the ceiling and the two opposite lateral walls are maintained at the temperature of the inlet jet temperature, T_c. The air properties at the reference temperature $T_{mean} = 298$ K are respectively $\rho_{air} = 1.2$ kg m^{-3} for density, $\nu_{air} = 1.5 \times 10^{-5}$ m^2 s^{-1} for the kinematic viscosity, $\kappa_{air} = 2.1 \times 10^{-5}$ m^2 s^{-1} for the thermal diffusivity. In these conditions, the value of the Prandtl number is $Pr = 0.71$ and the Rayleigh number based on the cavity height is equal to $Ra_H = 2.4 \times 10^9$.

The flow rate velocity at the inlet U_{inj} can be varied from 0.2 m s^{-1} to 0.6 m s^{-1}. The corresponding Reynolds number based on the height on the inlet slot, Re_h varies from 240 to 720 and the Froude number based on the inlet height, $Fr_h = U_{inj}/\sqrt{g\beta h\Delta T}$ lies in the range $1.84 < Fr_h < 5.51$.

The maximum turbulent kinetic energy, k, measured at the inlet was equal to 1.25×10^{-3} m^2 s^{-2} and corresponds to a turbulence intensity, I_t, of 6%.

Radiative heat transfer between the walls are eliminated by imposing isothermal conditions on the four active walls, and due to the thermal guard cavities, the front and rear walls can be considered adiabatic.

5.2. Airflow behaviour

Depending on the relative balance between the different forces acting on the inlet jet, two main flow patterns have been experimentally observed in this cavity. At relatively high Froude number values, the main feature of the flow consists in a general clockwise circulation with a small counter-clockwise recirculation cell located under the base of the inlet jet. As the jet emerging in the cavity is colder than the surrounding fluid, the buoyant force is thus directed downwards. The initial jet inertia combined with the ascending pressure gradient caused by the Coanda effect due to the ceiling are in this case sufficient to overcome the Archimede force and the jet penetrates horizontally in the cavity, more or less according to the evolution of the relative strength of the antagonistic forces. The second airflow pattern is encountered at low Froude number values. The jet momentum and the Coanda effect are in this case no more sufficient to overcome the buoyant force. The inlet jet thus separates from the ceiling and flows downwards along the vertical wall, then along the bottom wall to the exhaust slot, resulting in a counter-clockwise general flow. Moreover, a singular behaviour was also experimentally when varying the inlet jet velocity. When decreasing U_{inj} from an initial clockwise flow, the change to a counter-clockwise situation was observed for a critical Fr_h value. At the opposite, when starting from a counter-clockwise flow and

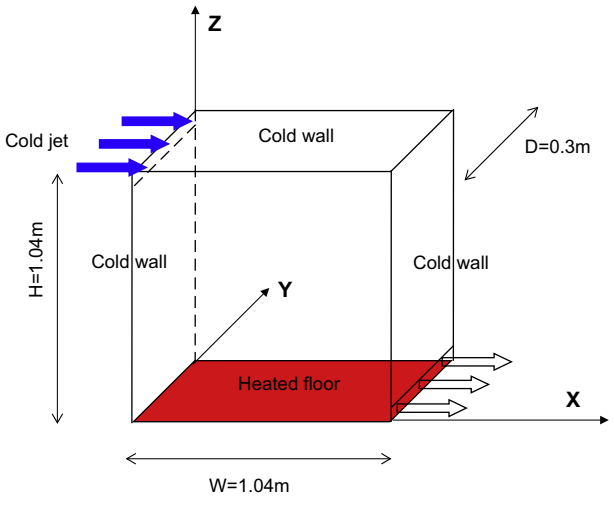

Fig. 1. Schematic representation of the experimental cavity.

increasing U_{inj}, the clockwise pattern was recovered, but for a higher Fr_h value than the preceding one. This means that the flow bifurcation from one general rotation to the opposite one is associated to a hysteresis phenomenon and consequently that this flow bifurcation is probably of subcritical nature.

In the experiments, the counter-clockwise situation was always observed below $Fr_h = 2.02$ and the clockwise flow was recovered above $Fr_h = 3.58$.

6. Numerical methodology

In this context, we chose to investigate numerically the complex and numerically challenging airflow developed in this slot-ventilated heated cavity with an LES approach laid on the dynamic version of the Mixte Scale Diffusivity Model described above.

The goal of the study is in fact twofold. First, check the validity of the MDSM model in mixed convection flow situations by comparison not only with the experimental database but also with the dynamic Germano–Lilly procedure, which is the more widely used subgrid-scale model and can therefore be considered as the reference subgrid model for LES. This later point will be achieved through comparison with Zhang et al.'s recent results [5], as these authors employed the dynamic Germano–Lilly model. The second objective is to tackle the bifurcation phenomenon and the observed hysteresis cycle.

As a dynamic procedure is used here to locally adjust the value of the subgrid model constant, a clipping must be done in order to prevent unrealistic negative values of the diffusivity. Nevertheless, various numerical tests enable us to observe that authorising weak negative values of the subgrid diffusivity slightly improves the quality of the results. As a consequence, we impose $\kappa_{sm} \geq -0.1\kappa_{mol}$ instead of a stricter $\kappa_{sm} \geq 0$ condition.

Two different meshes are used in order to test the grid dependence of the results. First we consider a $60 \times 10 \times 60$ grid along respectively the width, depth and height of the cavity. This grid will be hereafter denoted G1, and is similar to the spatial resolution employed by Zhang and Chen [4] ($62 \times 12 \times 62$) and Zhang et al. [5] ($60 \times 30 \times 60$). In our case, four points are located along the vertical direction into the inlet and into the outlet slots. A smooth tangent-hyperbolic law is applied for the distribution along the X, Y and Z directions in order to refine the mesh near the walls as well as inside the inlet and the outlet regions.

The position of the first inner grid point in the X direction is 9.26×10^{-3} in non-dimensional units. The corresponding values in terms of walls units y^+ for $U_{inj} = 0.33$ m s^{-1} are 8 for the clockwise flow situation and 11.6 for the counter-clockwise pattern. Along the Z axis, the first inner point is located at $z = 3.39 \times 10^{-3}$. The corresponding y^+ values are respectively 4.7 (clockwise) and 7.1. The last point is at a distance $d = 2.506 \times 10^{-3}$ of the ceiling, and y^+ equals 1.2 for an anti-clockwise general flow and 5.5 for a clockwise flow.

The second mesh (G2) is a finer $96 \times 34 \times 96$ grid points with seven points into the inlet slot and 11 points inside the outlet slot.

We must mention that in both cases, no wall function is applied to the subgrid model as it naturally vanishes at the wall.

The inlet velocity distribution is imposed with respect to the measured velocity profile, with a fitted parabolic distribution along the vertical direction and a uniform profile along the spanwise direction as:

$$u(x = 0, 0 < y < A_Y, 1 - h/H < z < 1) = -4340.4z^2 + 8608.2z - 4267 \quad (13)$$

and satisfies $(H/h)\int_{1-h/H}^{1} u(z)\mathrm{d}z = 1$. Moreover, in order to account for the experimental turbulent intensity, a white noise perturbation can be superimposed to the inlet velocity profile. At the outlet, the normal derivatives are set to zero for all the variables.

The time step is set to 0.003 in non-dimensional units, and the statistics of the flow have been established over a period of at least 180 non-dimensional time units, which proved to be enough for obtaining converged statistics.

7. Results

7.1. Test case $U_{inj} = 0.57\ m\,s^{-1}$

We first consider the case $U_{inj} = 0.57$ m s^{-1} in order to check the validity of our LES approach for mixed convection flow situations. The values of the non-dimensional parameters in this case are respectively $Ra_H = 2.4 \times 10^9$ for the Rayleigh number, $Re_h = 684$ for the Reynolds number and $Fr_h = 5.24$ for the Froude number. This situation corresponds to an observed clockwise flow pattern.

We compare the present LES results not only with the experimental results [6–8] but also with the LES results of the recent comparative study of different CFD approaches carried out by Zhang et al. [5]. These authors used FLUENT® commercial code for their simulations and a Germano–Lilly dynamic approach for their LES results on a $60 \times 30 \times 60$ grid points mesh. Following the experimental available data, only the median plane of the cavity ($y = 0.5 \times A_y = 0.15$) will be considered and we choose to present the results using the inlet jet Froude number, Fr_h, as done in Refs. [7] and [8].

Fig. 2 presents the vertical profiles of the mean horizontal velocity, temperature and turbulent kinetic energy at mid-width of the cavity ($x = 0.5$); while horizontal profiles of the mean vertical velocity, temperature and turbulent kinetic energy at mid-height ($z = 0.48$) are reported in Fig. 3.

Let us first consider the influence of the spatial resolution comparing the LES results obtained for the two grids previously described, G1 and G2. The results obtained on the coarse grid G1 agree well with those of the refined grid G2, particularly for the vertical and horizontal temperature distributions (Figs. 2(b) and 3(b)). Slight differences can be observed on the vertical and horizontal profiles of the velocity in the central core of the cavity, but the respective velocity peak values near the walls are very close (Figs. 2(a) and 3(a)). The turbulent kinetic energy profiles in Figs. 2(c) and 3(c) experience the same general shapes on the two grids, but the lower values obtained in the central region of the cavity for grid G2 are in better agreement with the experimental data. This comparison shows, however, that the spatial resolution of grid G1 is enough for correctly describing the flow encountered in this cavity.

Let us now focus on the comparison with the experimental data and the LES data of Zhang et al. Generally speaking, the LES results are in a pretty good agreement with the experimental data and the general trends of the mean fields are correctly predicted. Particularly, both LES are able to reproduce the fact that the core of the cavity remains almost isothermal (Fig. 2(b)), and the agreement with the vertical experimental temperature profile is excellent. The core temperature is 19.6 °C for G1 and 19.5 °C for G2 while the measured value is 19.4 °C.

Some differences can, however, be observed between our LES results and those of Zhang et al.'s If we compare the vertical profiles of the horizontal velocity in Fig. 2(a), Zhang et al. LES predict a very narrow ceiling jet. On the other hand, our results present a spread jet in accordance to the experimental one, with however a slight over-prediction of the peak velocity value. Our LES also better describes the return flow near the floor of the cavity. When examining now the horizontal profiles of the vertical velocity (Fig. 3(a)), the present LES better agrees with the experimental data in the first part of the profile ($x < 0.5$), while Zhang et al.'s LES better fits the experimental data in the second part. The maximum values in the vertical boundary layers are, however, well predicted by our LES.

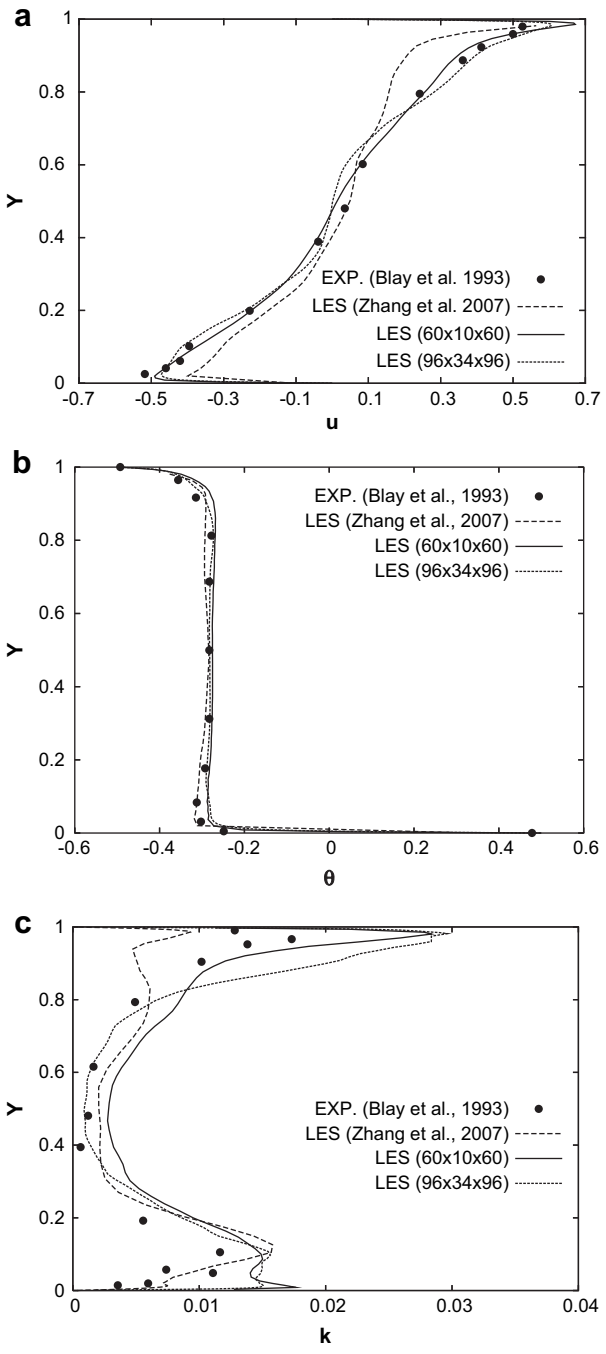

Fig. 2. Comparison of LES results with the experiment data at cavity mid-width ($x = 0{,}5$) in the median plan ($y = 0{,}15$): (a) mean horizontal velocity, (b) mean temperature, (c) turbulent kinetic energy. $Ra_H = 2.4 \times 10^9$ and $Fr_h = 5.24$.

The comparison of the horizontal temperature profile at mid-height (Fig. 3(b)) is also correct, but our LES tends to slightly over-predict the temperature level compared to [5].

If we now consider the turbulent quantities on Figs. 2(c) and 3(c), we observe that the turbulence is quite low in the central part of the cavity but significant near the walls and corresponds to a main flow encircling the isothermal and quiet core region. The current LES results reproduce the evolution of the experimental profiles, but generally over-predict the turbulence level, while Zhang et al.'s profiles are not in a good agreement with the experimental ones near the vertical walls and in the jet area.

As a conclusion of this part, it appears that the subgrid diffusivity model used in this study compares well with the classical Germano–Lilly dynamic model. Moreover, it proves to correctly reproduce the mean flow characteristics in the experimental cavity even on a coarse grid and, as a consequence, is well suited for mixed convection flow problems in cavities.

7.2. Flow bifurcation and hysteresis

During experimental visualizations reported in [6], a great sensitivity of the flow structure to the Froude number was observed

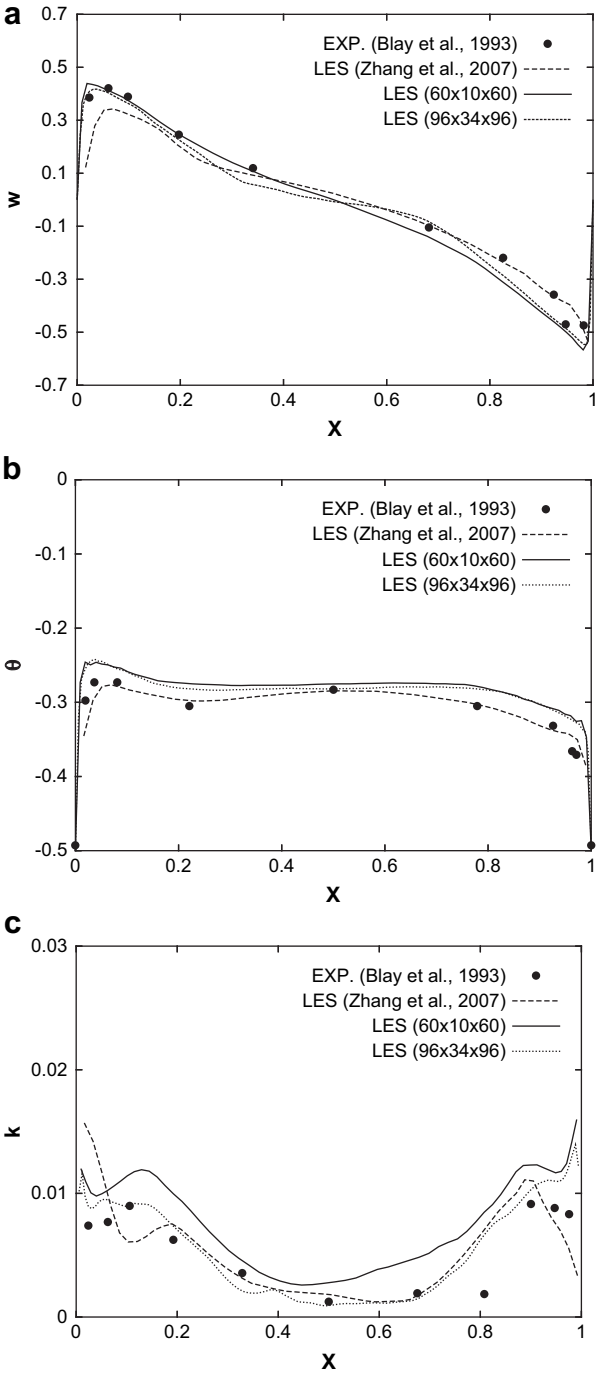

Fig. 3. Comparison of LES results with the experiment data at cavity mid-height ($z = 0.48$) in the median plan ($y = 0.15$): (a) mean horizontal velocity, (b) mean temperature and (c) turbulent kinetic energy. $Ra_H = 2.4 \times 10^9$ and $Fr_h = 5.24$.

Table 1
Comparison between the experimental and the numerical main stream rotation (EXP, experimental data; LES, LES without inlet flow perturbation; LES-pert, LES with inlet flow perturbation).

U_{inj} (m s^{-1})	Re_h	Fr_h	Decreasing phase		Increasing phase		
			EXP	LES/ LES-pert	EXP	LES	LES-pert
0.6	720	5.51	+	+			
0.57	684	5.24	+	+	+	+	+
0.50	600	4.59	+	+	+	−	+
0.39	468	3.58	+	+	+	−	−
0.33	396	3.03	+	+	−	−	−
0.28	336	2.57	+	+	−	−	−
0.22	264	2.02	−	−	−	−	−
0.2	240	1.84	−	−	−	−	−

and revealed the existence of a flow bifurcation characterized by a critical Froude number around which the overall stream can vary from a clockwise rotation (hereafter noted +), to a counter-clockwise rotation (hereafter noted −). It appeared also that for a given set of parameters, a significant hysteresis effect exists because the main rotation could be clockwise or counter-clockwise, depending on the initial state of the flow.

Table 1 reports the different experimental conditions considered in [6] with the corresponding Froude numbers and the observed flow rotation (+ or −).

Numerically, an example of the double solution observed for a set of parameters $Ra_H = 2.4 \times 10^9$ and $Fr_h = 3.03$, is given in Fig. 4, where the two main stream rotations obtained with our LES computations are reported. Fig. 4 shows that the simulations capture all the features of the flow pattern observed in the experiments for the clockwise and counter-clockwise situations. Especially for the clockwise case (Fig. 4, left), the small recirculation cell observed close to the inlet jet in the experiments is well reproduced.

The flow pattern obviously influences the heat transfer at the walls. So, for the clockwise situation the mean Nusselt number along the central line of the floor ($y = 0.15$) is equal to 141.8, but is enhanced when the cold jet directly flows downwards the heated floor (anti-clockwise rotation) and the value in this case is 152.4.

Lastly, in order to numerically reproduce the hysteresis phenomenon, the following procedure was adopted: starting from

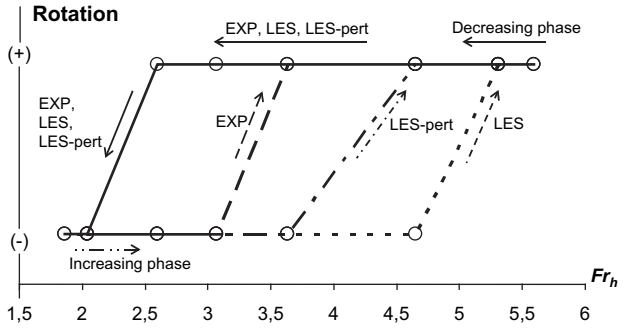

Fig. 5. Comparison between the experimental and the numerical hysteresis cycles. (+) Stands for a clockwise main flow and (−) for a counter-clockwise main flow. The circles correspond to experimental or numerical points, with respect to the tabulated values of Table 1.

a given Froude number such as the general stream is flowing in the clockwise direction, the inlet jet velocity is gradually decreased until a counter-clockwise rotation is reached. This consists in the decreasing phase. The first value for which the change in rotation appears is $Fr_h^{(-)}$. Then, starting from this new initial counter-clockwise state, the inlet velocity is gradually increased (increasing phase), passing through the same Fr_h values than those considered in the decreasing phase. The first value for which the rotation changes in sign is $Fr_h^{(+)}$. Two different conditions were used at the inlet: in the first case, no random noise was considered for the inlet velocity, while a random noise consistent with the observed turbulent intensity was imposed in the second case. The directions of the flow are reported in Table 1 and the corresponding numerical hysteresis cycles are plotted in Fig. 5, as well as the experimental cycle. We can observe first that the present LES is able to reproduce with a very good agreement the change between the clockwise and counter-clockwise rotation during the decreasing phase, whether the perturbation at the inlet is imposed or not. $Fr_h^{(-)}$ in this case is equal to 2.02. The reestablishment of the clockwise rotation is also observed numerically, but for a Froude number $Fr_h^{(+)}$ different from the experimental one. We can also notice the great influence of the inlet velocity conditions on the transition between the two flow regimes. Without any velocity fluctuations at the inlet, $Fr_h^{(+)}$ is equal

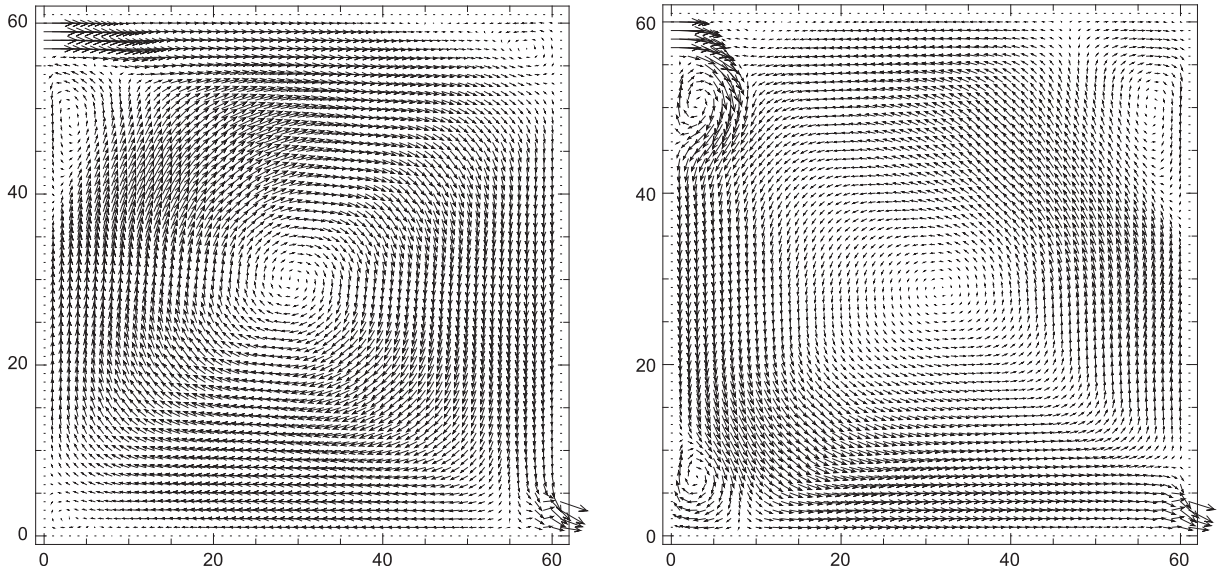

Fig. 4. Existence of a double solution: mean velocity fields for the same parameters set, $Ra_H = 2.4 \times 10^9$ and $Fr_h = 3.03$. Clockwise rotation (left) and counter-clockwise rotation (right). For clarity of the figures, the grid points are regularly distributed.

to 5.24, but when a random noise is added, this value reduces to 4.59, which is however higher than the experimental $Fr_h^{(+)} = 3.58$ value.

8. Conclusion

We used in this study an LES approach based on a diffusivity model that was initially developed for natural convection problems. This model proves to be also efficient in the mixed flow configuration encountered in the ventilated anisothermal cavity considered here. First, the mean features of the flow and the hysteresis cycle associated with a subcritical bifurcation inducing a change in direction of the general flow pattern in the cavity are well reproduced compared to existing experimental data. This, to our knowledge, has never been reported in the literature before. Further investigations are however necessary to improve the transition from the buoyant descending flow situation to the inertial horizontal jet flow regime. Particularly, the numerical bifurcation between the two flow structures proves to be very dependent on the turbulence level at the inlet, so development of more realistic conditions for the velocity fluctuations at the inlet are needed.

Acknowledgments

The authors greatly thank Dr. Zhao Zhang for providing a wide set of his numerical data.

References

[1] P.V. Nielsen, Specification of a two-dimensional test case, IEA Annex 20, Research Item 1.45. Report ISSN 0902-7513 R9040, Department of Building Technology and Structural Engineering, Aalborg, 1990.
[2] L. Davidson, P.V. Nielsen, Large Eddy simulation of the flow in a three-dimensional ventilated room, , In: Proceedings of the Fifth International Conference on Air distribution in Rooms, Roomvent '96, vol. 2 (1996) 161–168.
[3] Q. Chen, Prediction of different k-ϵ models for indoor airflow configurations, Numerical Heat Transfer B 28 (1995) 353–369.
[4] W. Zhang, Q. Chen, Large eddy simulation of natural and mixed convection airflows indoors with two simple filtered dynamic subgrid-scale models, Numerical Heat Transfer A 37 (2000) 447–463.
[5] Z. Zhang, W. Zhang, Z. Zhai, Q. Chen, Evaluation of various turbulence models in predicting airflow and turbulence in enclosed environments by CFD: part 2 – comparison with experimental data from literature, HVAC&R Research 13 (6) (2007) 871–886.
[6] S. Mergui, Caractérisation expérimentale des écoulements d'air de convection naturelle et mixte dans une cavité fermée, thèse de l'Université de Poitiers, France, 1993.
[7] D. Blay, S. Mergui, C. Niculae, Confined turbulent mixed convection in the presence of a horizontal buoyant wall jet, Fundamentals of Mixed Convection, HTD 213 (1992) 65–72.
[8] D. Blay, S. Mergui, J.L. Tuhault, F. Penot, Experimental turbulent mixed convection created by confined buoyant wall jets. In: First Eur Heat Transf Conf, UK, Sept 1992, pp. 821–828.
[9] W. Xu, Q. Chen, A two-layer turbulence model for simulating indoor airflow. Part II. Applications, Energy and Buildings 33 (2001) 627–639.
[10] J. Smagorinsky, General circulation experiments with the primitive equations I: the basic experiment, Monthly Weather Review 91 (3) (1963) 99–165.
[11] M. Germano, U. Piomelli, P. Moin, W.H. Cabot, A dynamic subgrid-scale eddy viscosity model, Physics of Fluids A3 (1991) 1760–1765.
[12] D.K. Lilly, A proposed modification of the Germano subgrid-scale closure model, Physics of Fluids 4 (1992) 633–635.
[13] A. Sergent, P. Joubert, P. Le Quéré, Development of a local subgrid diffusivity model for large eddy simulation of buoyancy driven flows: application to a square differentially heated cavity, Numerical Heat Transfer A 44 (8) (2003) 789–810.
[14] J. Salat, S. Xin, P. Joubert, A. Sergent, F. Penot, P. Le Quéré, Experimental and numerical investigation of turbulent natural convection in a large air-filled cavity, Integer Journal of Heat Fluid Flow 25 (5) (2004) 824–832.
[15] A. Sergent, P. Joubert, P. Le Quéré, Surface radiation effects on turbulent Rayleigh-Bénard convection in a parallelepipedic cavity, in: K. Hanjalić, Y.N. Jakirlić (Eds.), Proceedings of Turbulence, Heat and Mass Transfer, 5, 2006, pp. 531–534.
[16] J. Bardina, J. Ferziger, W. Reynolds, Improved subgrid-scales models for large eddy simulation, AIAA Paper (1980) 80-1357.